Journal of Sound and Vibration (1997) **199**(1), 1–15

STABILITY OF A JOINTED FREE-FREE BEAM UNDER END ROCKET THRUST

K. A. Mladenov

University of Architecture, Civil Engineering and Geodesy, Engineering Mechanics Division, 1 Hristo Smirnenski Boulevard, Sofia-1421, Bulgaria

AND

Y. Sugiyama

Department of Aerospace Engineering, College of Engineering, Osaka Prefecture University, 1-1, Gakuen-cho, Sakai, Osaka 593, Japan

(*Received* 3 *October* 1995, *and in final form* 1 *April* 1996)

This paper deals with the stability of a flexible space structure subjected to an end rocket thrust. The thrust acts upon the structure as a follower non-conservative force, thus the structure can lose its stability by flutter or divergence depending on the system parameters. It is assumed that the articulated free-free beams are subjected to a tangential follower force. The model consists of two viscoelastic beams interconnected by two kinds of joints. One of the joints is composed of a rotational viscoelastic spring while another is a shear viscoelastic spring. A FEM formulation of the articulated structure is performed. Bending flutter or post-flutter divergence are shown to occur depending on the joint rigidity and the internal damping.

1. INTRODUCTION

Free-free beams have been intensively exploited to simulate the stability behaviour of flexible missiles and/or space structures propelled by end rocket thrust [1–8]. Beal's paper [1] deals with a uniform beam under constant and pulsating thrust including a simplified control system. Matsumoto and Mote [2] have taken into account the effect of a finite time delay in the control mechanism. Park and Mote [3] have studied a similar problem with emphasis on the location and the inertia of a concentrated mass, the location of the follower force direction control sensor, the sensor gain and the maximum thrust magnitude allowable for stable planar motion. Wu's papers [5–7] are concerned with some interesting features of missiles with and without feedback control. The destabilizing effect of small material damping is demonstrated by Sugiyama and his collaborators [8]. On the other hand, a method of determining natural frequencies and mode shapes of free-free beams from the experimental data of the corresponding constrained structures is dealt with by Chen *et al*. [9].

Due to the non-conservative nature of the end thrust a consistent dynamic analysis is needed to correctly predict the stability behaviour [10–12].

2. PROBLEM STATEMENT AND SOLUTION

2.1. MATHEMATICAL MODEL

The jointed space structure under consideration, subjected to an end rocket thrust, is represented by a simple model of jointed free-free beams, as shown in Figure 1. The joint between the two viscoelastic beams consists of a spring K_r and a dashpot C_r related to the

0022–460X/97/010001 + 15 $25.00/0/sv960625

rotational motion, and a spring K_s together with a dashpot C_s connected with the shear motion. The dimension of the joint itself is assumed to be small and is neglected. The co-ordinate along the length of the beam is denoted by z while u stands for the lateral displacement of the section-z. The entire structure is formed by two identical beams, each one with a bending stiffness EI (E—Young's modulus of elasticity, I—second area moment of inertia) and having the Sezawa coefficient of visco-elastic resistance E^* (see [13]). Force P is assumed constant as far as its magnitude is concerned, otherwise its line of action varies, remaining always tangent to the elastic line at the tail cross-section.

Aerodynamic forces are disregarded in this study and simple beam theory is applied.

2.2. METHOD OF ANALYSIS

The extended Hamilton's principle can be written as

$$\delta \int_{T_1}^{T_2} (T + V + W_c)\,\mathrm{d}t + \int_{t_1}^{t_2} \delta W_{nc}\,\mathrm{d}t = 0, \tag{1}$$

where t is the time co-ordinate. Also, for the model in Figure 1, the kinetic energy T, the elastic potential energy V, the work W_c done by the conservative component of the thrust and the virtual work δW_{nc} done by the non-conservative forces, are determined as follows:

$$T = \tfrac{1}{2}\int_0^L m u_t^2\,\mathrm{d}z,$$

$$V = \tfrac{1}{2}\int_0^L EI u_{zz}^2\,\mathrm{d}z + \tfrac{1}{2}K_r[u_z|_{z=z_b} - u_z|_{z=z_f}]^2 + \tfrac{1}{2}K_s[u|_{z=z_b} - u|_{z=z_f}]^2,$$

$$W_c = \tfrac{1}{2}\int_0^L \frac{P}{L} u_z^2\,\mathrm{d}z, \tag{2}$$

where

$$\delta W_{nc} = \delta W_{ncf} + \delta W_{ncd}, \qquad \delta W_{ncf} = -P u_z|_{z=L}\delta u|_{z=L},$$

$$\delta W_{ncd} = \int_0^L E^* I u_{tzz}\delta u_{zz}\,\mathrm{d}z - C_r[u_{tz}|_{z=z_b} - u_{tz}|_{z=z_f}]\delta[u|_{z=z_b} - u|_{z=z_f}]$$

$$- C_s[u_t|_{z=z_b} - u_t|_{z=z_f}]\delta[u|_{z=z_b} - u|_{z=z_f}].$$

δW_{ncf} is the non-conservative virtual work of the thrust whereas δW_{ncd} is due to the viscoelastic properties of the beams and joints. Differentiation with respect to t and z are

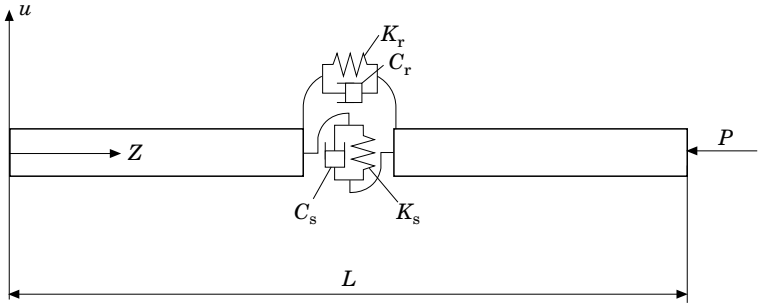

Figure 1. The free-free model.

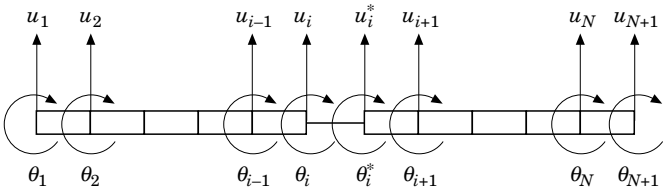

Figure 2. The displacement vectors and angles of rotation.

denoted by subscripts, while z_b and z_f stand for the tip of the rear beam and the downstream end of the front beam, respectively.

For simplicity the following dimensionless quantities are introduced:

$$\xi = z/L, \qquad \xi_b = z_b/L, \qquad \xi_f = z_f/L, \qquad \tau = t/L^2\sqrt{m/EI}, \qquad Q = PL^2/\pi^2 EI,$$

$$\gamma = (E^*/EL^2)\sqrt{EI/m}, \qquad \kappa_r = K_r L/EI, \qquad \kappa_s = K_s L^3/EI,$$

$$\delta_r = (C_r/EIL)\sqrt{EI/m}, \qquad \delta_s = (C_s L/EI)\sqrt{EI/m}. \tag{3}$$

Substitution of equations (2) and (3) into equation (1), after transformations, leads to

$$\delta \int_{\tau_1}^{\tau_2} \left\{ \int_0^1 \tfrac{1}{2}u_\tau^2 \, \mathrm{d}\xi - \int_0^1 \tfrac{1}{2}u_{\xi\xi}^2 \, \mathrm{d}\xi - \tfrac{1}{2}\kappa_r [u_\xi|_{\xi=\xi_b} - u_\xi|_{\xi=\xi_f}]^2 - \tfrac{1}{2}\kappa_s [u|_{\xi=\xi_b} - u|_{\xi=\xi_f}]^2 \right\} \mathrm{d}\tau$$

$$- \delta \int_{\tau_1}^{\tau_2} \left\{ \tfrac{1}{2} \int_0^1 \pi^2 Q \xi u_\xi^2 \, \mathrm{d}\xi \right\} \mathrm{d}\tau$$

$$- \int_{\tau_1}^{\tau_2} \{ \pi^2 Q u_\xi|_{\xi=1} \delta u|_{\xi=1} + \delta_r [u_{\tau\xi}|_{\xi=\xi_b} - u_{\tau\xi}|_{\xi=\xi_f}] \delta [u_\xi|_{\xi=\xi_b} - u_\xi|_{\xi=\xi_f}] \} \, \mathrm{d}\tau$$

$$- \int_{\tau_1}^{\tau_2} \left\{ \delta_s [u_\tau|_{\xi=\xi_b} - u_\tau|_{\xi=\xi_f}] \delta (u|_{\xi=\xi_b} - u|_{\xi=\xi_f}) + \int_0^1 \gamma u_{\tau\xi\xi} \delta u_{\xi\xi} \, \mathrm{d}\xi \right\} \mathrm{d}t = 0. \tag{4}$$

Differentiation with respect to the non-dimensional independent variables τ and ξ have been denoted by the corresponding subscripts.

The mechanical system under consideration is divided into N equal finite elements, as shown in Figure 2. The vector $\mathbf{V}$ of the displacements and slope angles for the entire structure is

$$\mathbf{V} = \{u_1, \theta_1, u_2, \theta_2, \ldots, u_i, \theta_i, u_i^*, \theta_i^*, \ldots, u_{N+1}, \theta_{N+1}\}^{\mathrm{T}}. \tag{5}$$

The displacement field within an element is assumed to be

$$\mathbf{u}(\xi, \tau) = \mathbf{a}(\xi)\mathbf{v}(\tau) \tag{6}$$

where

$$\mathbf{a}(\xi) = \{(1-\xi)^2(1+2\xi), \xi(1-\xi)^2/N, \xi^2(3-2\xi), \xi^2(1-\xi)/N\} \tag{7}$$

is the well-known shape function, and $\mathbf{v}(\tau)$ is the vector of the nodal displacements.

Substitution of equation (6) into equation (4) yields, upon transformations, a matrix

equation for the entire structure

$$\mathbf{M}\mathbf{V}_{\tau\tau} + \mathbf{C}\mathbf{F}_{\tau} + \mathbf{K}\mathbf{V} = \mathbf{0}. \tag{8}$$

Here, $\mathbf{M}$ is the mass matrix with elements $\mathbf{M}^{(i)}$, $\mathbf{C}$ is the dissipation matrix consisting of $\mathbf{C}^{(i)}$, $\mathbf{C}_{D1}$ and $\mathbf{C}_{D2}$ submatrices (the last one being related to the joint dissipation). Also $\mathbf{K}$ is the stiffness matrix formed by the submatrices $\mathbf{K}_1^{(i)}$, $\mathbf{K}_2^{(i)}$, $\mathbf{L}_1^{(N_s-N)}$, $\mathbf{K}_{S1}$, and the joint stiffness matrix $\mathbf{K}_{S2}$. The constituent submatrices are given in the appendix.

The displacement field varies with time according to an exponential law, namely

$$\mathbf{V}(\tau) = \mathbf{V}_0 \exp(S\tau), \qquad \mathbf{V}_1 = S\mathbf{V}_0. \tag{9}$$

From (8) and (9) one gets

$$\mathbf{A}\tilde{\mathbf{V}} = S\tilde{\mathbf{V}}, \qquad \mathbf{A} = \begin{bmatrix} \mathbf{0} & \mathbf{I} \\ -\mathbf{M}^{-1}\mathbf{K} & -\mathbf{M}^{-1}\mathbf{C} \end{bmatrix}, \qquad \tilde{\mathbf{V}} = \begin{Bmatrix} \mathbf{V}_0 \\ \mathbf{V}_1 \end{Bmatrix}. \tag{10}$$

In this way the eigenvalue problem is reduced to analyzing the features of the eigenvalues and the corresponding eigenvectors.

3. RESULTS AND DISCUSSION

The investigation of stability of the free-free beam has been carried out through the features of the root loci in the complex S-plane. In the present study the internal damping (both material dissipation within the beams and internal damping at the joint) has been taken into account. The calculations have been performed for $N = 8$ finite elements. The joint is located at the center of the structure.

3.1. EIGENMODES

Figure 3 represents four typical fundamental eigenmodes for $Q = 0$, $\kappa_r = \kappa_s = 10^2$, $\delta_r = 0{\cdot}01$, $\delta_s = 1{\cdot}0$, and $\gamma = 0$. Figures 3(a) and 3(b) show translational and rotational rigid body motions, respectively, while Figures 3(c) and 3(d) depict the first and the second bending motions.

3.2. SEVERAL TYPES OF INSTABILITY

In this section the instability of the beam is investigated depending on the variation of the joint stiffness parameters κ_r and κ_s. In fact, it is assumed that the joint is relatively rigid with respect to shear deformation. That is why relatively large values of 10^4, 10^3 and 10^2 have been taken for κ_s, whereas κ_r is varied within the range $10^0 - 10^4$. The remaining

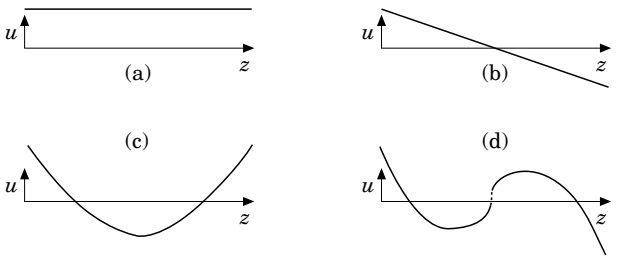

Figure 3. Some representative eigenmodes ($\kappa_r = \kappa_s = 10^2$, $\delta_r = 0{\cdot}1$, $\delta_s = 1{\cdot}0$, $\gamma = 0$): (a) rigid-body translation; (b) rigid-body rotation; (c) first bending mode; (d) second bending mode.

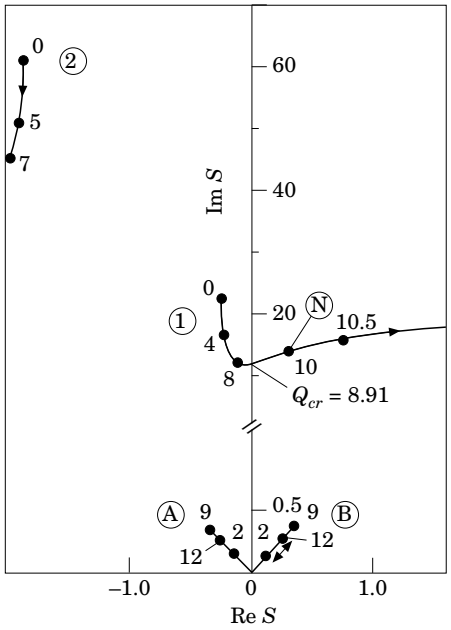

Figure 4. Root loci ($\kappa_r = \kappa_s = 10^4$, $\delta_r = 0{\cdot}1$, $\delta_s = 1{\cdot}0$, $\gamma = 0{\cdot}001$).

parameters, namely $\delta_r = 0{\cdot}1$, $\delta_s = 1{\cdot}0$ and $\gamma = 0{\cdot}001$, are kept fixed. This data gives rise to several types of instability.

Consider first the standard case of the structure equipped with stiff bending and shearing springs, that is $\kappa_r = \kappa_s = 10^4$. Figure 4 ($\kappa_r = \kappa_s = 10^4$, $\delta_r = 0{\cdot}1$, $\delta_s = 1{\cdot}0$ and $\gamma = 0{\cdot}001$) depicts some typical root loci versus the loading parameter Q in the complex plane with a real horizontal Re S-axis and an imaginary vertical Im S-axis. The branches **1** and **2** indicate the first and the second bending vibration modes, respectively, while the branches **A** and **B** correspond to rigid body modes. To begin with, consider branch **1**. Increasing Q above 8·91 results in eigenvalues with positive real part. That is why this value is the flutter critical force, i.e. $Q_{cr} = 8{\cdot}91$. At the same time the branch **2** is located in the stable domain. The branches **A** and **B** start from the origin for $Q = 0$. The branch **B**, being situated in the right-hand half-plane from the start, indicates flutter type of instability, which, however, is of a rigid-body translation mode. Rigid body motion does not cause structural damage. For this reason no critical force for rigid body modes will be specified here.

The case illustrated in Figure 4 is referred to as the first type (I) of instability. This type of instability can be characterized by the first bending mode flutter, together with inherent flutter in the rigid-body translation mode. Figure 5 depicts the type of motion performed by the structure in this type of instability. It is the first bending mode flutter at point **N** in Figure 4. Several eigenforms at different instances within a period are shown.

Secondly, consider the structure equipped with a soft rotational spring of $\kappa_r = 10^1$. Branch **1** in Figure 6 ($\kappa_r = 10^1$, $\kappa_s = 10^4$, $\delta_r = 0{\cdot}1$, $\delta_s = 1{\cdot}0$ and $\gamma = 0{\cdot}001$) shows that for Q exceeding 11·83 a flutter type instability occurs so that the corresponding flutter force is $Q_{cr} = 11{\cdot}83$. Branch **2** does not appear in this figure but it exists exactly in the stable (i.e. left-hand) region. Also, the branches **A** and **B** start from the origin for $Q = 0$. When afterwards Q is increased from zero, however, branch **B** enters into the right-hand half-plane. Then, for Q beyond 6·51 the root locus moves along the Im S-axis = 0, and

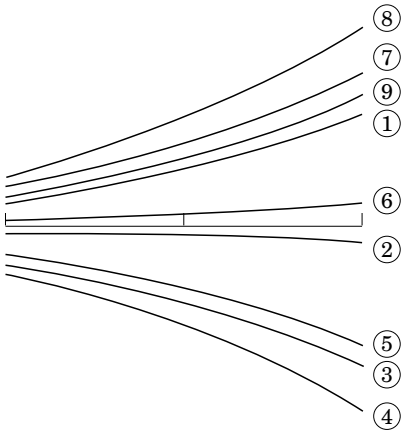

Figure 5. First bending mode flutter ($\kappa_r = 10^4$, $\kappa_s = 10^4$, $\delta_r = 0{\cdot}1$, $\delta_s = 1{\cdot}0$, $\gamma = 0{\cdot}001$, $Q = 10$, point **N** in Figure 4).

the real part of the root continues to increase in the positive direction. This type of instability will hereafter be called the Post-Flutter Divergence (for short PF divergence) with the notation $Q_{pf} = 6{\cdot}51$ as the PF divergence force. Since any dynamic method to control flutter does not effectively prevent divergence, PF divergence should be borne in mind by engineers involved with the present type of structural systems under an end follower thrust.

The case depicted in Figure 6 is referred to as type II instability. It is characterized by the appearance of PF divergence.

Thirdly, consider the structure equipped with a very soft rotational spring of $\kappa_r = 1{\cdot}0$. Observing Figure 7 ($\kappa_r = 1{\cdot}0$, $\kappa_s = 10^4$, $\delta_r = 0{\cdot}1$, $\delta_s = 1{\cdot}0$ and $\gamma = 0{\cdot}001$), we see that branch **2** yields the onset of flutter instability with a critical force $Q_{cr} = 11{\cdot}07$. Branch **1** is located in the stable half-plane. Branches **A** and **B** start from the origin for $Q = 0$. But if Q is

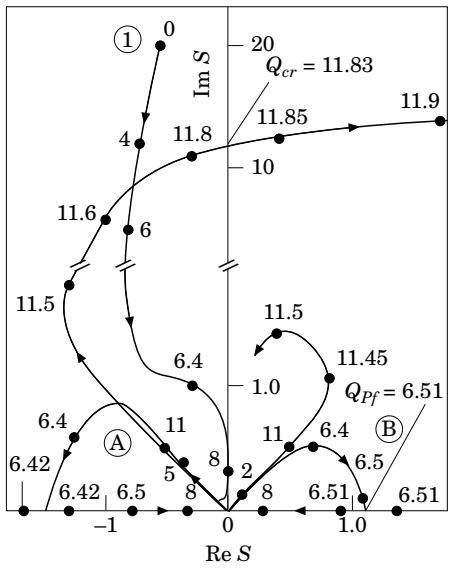

Figure 6. Root loci ($\kappa_r = 10^1$, $\kappa_s = 10^4$, $\delta_r = 0{\cdot}1$, $\delta_s = 1{\cdot}0$, $\gamma = 0{\cdot}001$).

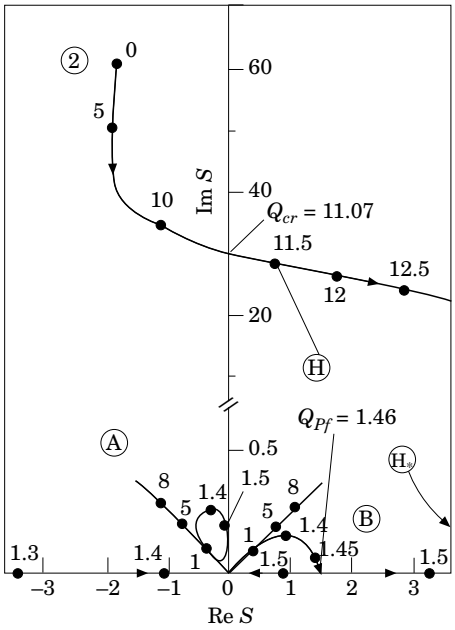

Figure 7. Root loci ($\kappa_r = 10^0$, $\kappa_s = 10^4$, $\delta_r = 0{\cdot}1$, $\delta_s = 1{\cdot}0$, $\gamma = 0{\cdot}001$).

increased, branch **B** shows PF-divergence instability with a critical value $Q_{pf} = 1{\cdot}46$. The case considered is designated as type III instability. It can be characterized by flutter in the second bending mode and PF divergence.

In order to help in understanding the physical aspect of type III instability, the second bending mode flutter at point **H** in Figure 7 is shown in Figure 8. Moreover, Figure 9 demonstrates post-flutter divergence instability at point $\mathbf{H}_*$ in Figure 7.

Finally, we consider the special case of the structure equipped with a soft rotational spring and a moderate shearing spring, that is $\kappa_r = 5$, $\kappa_s = 10^2$. Branch **B** in Figure 10 ($\kappa_r = 5$, $\kappa_s = 10^2$, $\delta_r = 0{\cdot}1$, $\delta_s = 1{\cdot}0$ and $\gamma = 0{\cdot}001$) shows a PF divergence instability

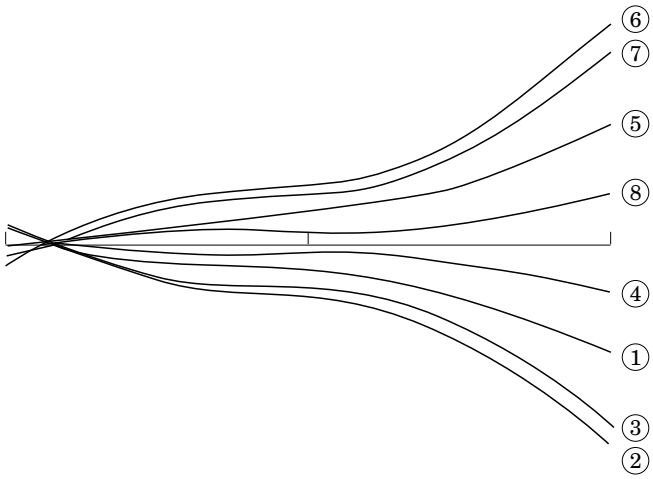

Figure 8. Second bending mode flutter ($\kappa_r = 10^0$, $\kappa_s = 10^4$, $\delta_r = 0{\cdot}1$, $\delta_s = 1{\cdot}0$, $\gamma = 0{\cdot}001$, $Q = 11{\cdot}5$, point **H** in Figure 7).

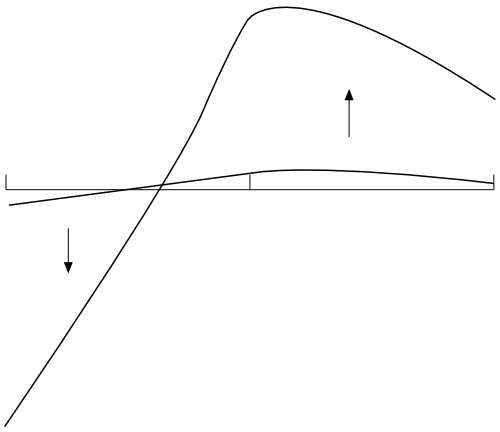

Figure 9. Post-flutter divergence ($\kappa_r = 10^0$, $\kappa_s = 10^4$, $\delta_r = 0{\cdot}1$, $\delta_s = 1{\cdot}0$, $\gamma = 0{\cdot}001$, $Q = 11$, point $\mathbf{H}_*$ in Figure 7).

pattern. The corresponding critical force is $Q_{pf} = 4{\cdot}86$. Branch **1** on the other hand, reaches the horizontal Im S-axis $= 0$, moves along it towards the right-hand half-plane, then coalesces with a branch of the trajectory **B** and enters the right-hand half-plane. This means flutter type instability for which the critical force parameter is $Q_{cr} = 6{\cdot}17$.

The case appearing in Figure 10 is type IV instability. The feature of this type of instability is that the locus for the first bending mode coalesces with the branch of the locus of the rigid-body motion and also the presence of PF divergence.

It turns out also that due to coalescence and transfer of two locus branches in the course of an increasing κ_r, branch form changes take place thus predicting various types of instability: first bending mode (branch **1**), second bending mode (branch **2**), and rigid-body motion (branch **A**). Figure 11 shows one such example where the solid lines are for $\kappa_r = 9$, $\kappa_s = 10^4$. The two trajectories with white dots have been obtained putting $\kappa_r = 9{\cdot}5$, $\kappa_s = 10^4$. By increasing κ_r slightly above 9·5 and keeping $\kappa_s = 10^4$, they coalesce and change the locus for $\kappa_r = 10$, $\kappa_s = 10^4$, as can be seen in Figure 6.

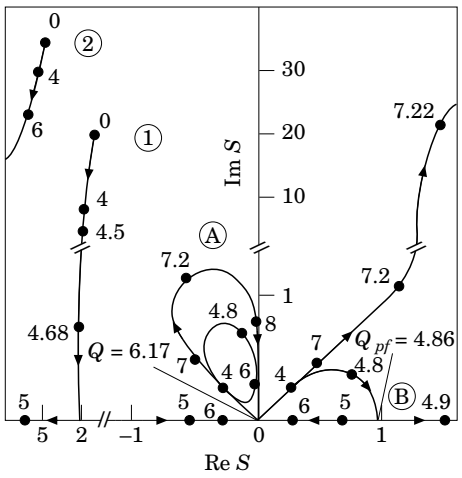

Figure 10. Root loci ($\kappa_r = 5$, $\kappa_s = 10^2$, $\delta_r = 0{\cdot}1$, $\delta_s = 1{\cdot}0$, $\gamma = 0{\cdot}001$).

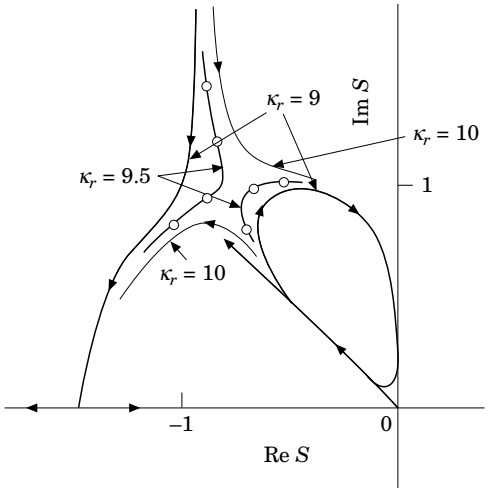

Figure 11. Branch evolution and transfer.

From the viewpoint of structural safety the aforementioned *three instability configurations* are important. On the contrary, the other root loci, located in the right-hand half-plane of the complex plane and corresponding to rigid-body translation modes, cannot cause structural damage. As for the critical forces, it seems relevant to consider the onset of structural damage itself.

It is worthwhile to note that the rigid-body-motion instability does not affect the system kinetics for the structure is supposedly stabilized by a control mechanism. This, however, is another problem and will not be treated in the present study.

3.3. EFFECT OF THE JOINT STIFFNESS ON INSTABILITY

Table 1 shows some critical forces and instability types versus κ_r and κ_s. When these parameters are relatively large, a flutter instability pattern of type I occurs. Note that the

TABLE 1

Types of instability and critical forces depending on joint stiffness

κ_s	κ_r						
	1·0	5·0	9·0	10^1	10^2	10^3	10^4
10^2	Type IV PFD 1·46 F 1·99	Type IV PFD 4·86 F 6·17	Type I F 6·02	Type I F 5·83	Type I 4·23	Type I 4·20	Type I 4·20
10^3	Type III PFD 1·46 F 10·62	Type III PFD 4·59 F 11·61	Type II PFD 6·25 F 11·42	Type II PFD 6·59 F 11·27	Type I 8·60	Type I 8·57	Type I 8·57
10^4	Type III PFD 1·46 F 10·7	Type III PFD 4·59 F 12·13	Type II PFD 6·19 F 11·98	Type II PFD 6·51 F 11·27	Type I 8·94	Type I 8·91	Type I 8·91

PFD: Post-flutter divergence, F: flutter

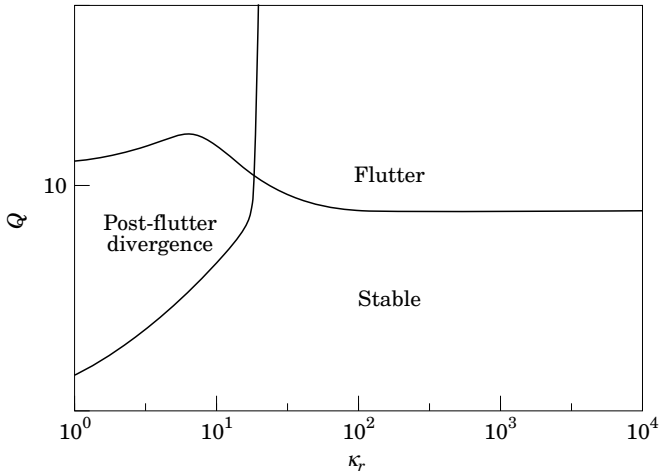

Figure 12. Stability limits ($\kappa_s = 10^4$).

critical force arises even for a small κ_r. On the other hand, when κ_s is small, the critical force declines. Thus, one concludes that κ_s should be kept large enough.

The instability patterns and critical forces in the case of a uniform free-free beam, that is, for large values of κ_r and κ_s (say $\kappa_r = \kappa_s = 10^4$), are dealt with in [8]. There, for instance, the first bending-mode-instability pattern appears for $Q_{cr} = 8{\cdot}95$. Results obtained for infinitely large κ_r and κ_s can be found in [8] too. A similar problem with considerably (even vanishing) smaller damping coefficients δ_r and δ_s was studied as well. This led to PF-divergence at extremely small critical forces. For this reason it was found not to be dangerous from a structural safety stand point.

It should be emphasized also that for $\kappa_s = 10$ the deflections of the front and the rear beams with respect to the joint appear to perform considerably differently. They, however, have been found to be stable by virtue of the stability criteria adopted in this paper. Relevant further analysis is to be carried out to reveal if these deflections could lead to structural damage. At this stage κ_s should be kept large enough.

A stability map Q versus κ_r for $\kappa_s = 10^4$ is given in Figure 12.

TABLE 2

Effect of δ_r and δ_s on flutter limit ($\kappa_r = \kappa_s = 10^4$, $\gamma = 0{\cdot}001$)

	δ_r			
δ_s	10^{-2}	10^{-1}	10^0	10^1
10^{-2}	8·91	8·91	8·91	8·92
10^{-1}	8·91	8·91	8·91	8·92
10^0	8·91	8·91	8·91	8·92
10^1	8·91	8·91	8·91	8·91

TABLE 3

Effect of δ_r and δ_s on flutter limit ($\kappa_r = 10^4$, $\kappa_s = 10^2$, $\gamma = 0{\cdot}001$)

δ_s	δ_r			
	10^{-2}	10^{-1}	10^{0}	10^{1}
10^{-2}	5·72	5·72	5·72	5·72
10^{-1}	5·40	5·40	5·40	5·40
10^{0}	4·20	4·20	4·20	4·20
10^{1}	4·48	4·48	4·48	4·49

TABLE 4

Effect of δ_r and δ_s on flutter limit ($\kappa_r = 10^2$, $\kappa_s = 10^4$, $\gamma = 0{\cdot}001$)

δ_s	δ_r			
	10^{-2}	10^{-1}	10^{0}	10^{1}
10^{-2}	8·87	8·94	9·54	10·36
10^{-1}	8·87	8·94	9·54	10·36
10^{0}	8·87	8·94	9·54	10·36
10^{1}	8·86	8·94	9·53	10·35

3.4. EFFECT OF THE JOINT INTERNAL DAMPING UPON INSTABILITY

Taking $\gamma = 0{\cdot}001$, the effect of the joint damping parameters δ_r and δ_s (varied within the interval 10^{-2}–10^{1}) upon flutter limit has been investigated. Some results for $\kappa_r = \kappa_s = 10^4$; $\kappa_r = 10^4$, $\kappa_s = 10^2$; $\kappa_r = 10^2$, $\kappa_s = 10^4$ are contained in Tables 2, 3 and 4. Type I instability appears for various values of δ_r and δ_s. When κ_r and κ_s are large, the critical forces do not seem to be influenced by δ_r and δ_s; but for a small κ_r, the magnitude of δ_r, and for a small κ_s, that of δ_s, can influence the corresponding critical forces considerably.

The results in Table 5 are obtained for $\kappa_r = 10^1$ and $\kappa_s = 10^4$. Instability types IV, II or III can occur depending on the magnitude of the damping parameter δ_r. At the same time δ_s does not affect the stability properties. It is confirmed that damping does not affect PF-divergence limit.

That is the way in which the joint internal damping in close connection with the joint stiffness exerts an influence upon the instability features of the free-free beams under consideration.

4. CONCLUSIONS

The present paper has discussed stability behaviour of free-free beams which consist of two visco-elastic modules interconnected by visco-elastic joints and subjected to a follower thrust at the tail end. The results lead to the following main conclusions:

TABLE 5

Types of instability and critical forces depending on damping ($\kappa_r = 10^1$, $\kappa_s = 10^4$, $\gamma = 0{\cdot}001$)

δ_s	δ_r			
	10^{-2}	10^{-1}	10^{0}	10^{1}
10^{-2}	Type IV PFD 6·48 F 8·36	Type II PFD 6·51 F 11·83	Type III PFD 6·76 F 11·25	Type III PFD 8·79 F 10·52
10^{-1}	Type IV PFD 6·48 F 8·36	Type II PFD 6·51 F 11·83	Type III PFD 6·76 F 11·25	Type III PFD 8·79 F 10·52
10^{0}	Type IV PFD 6·48 F 8·36	Type II PFD 6·51 F 11·83	Type III PFD 6·76 F 11·25	Type III PFD 8·79 F 10·52
10^{1}	Type IV PFD 6·48 F 8·36	Type II PFD 6·51 F 11·83	Type III PFD 6·76 F 11·25	Type III PFD 8·79 F 10·52

PFD: Post-flutter divergence, F: flutter

(1) The dependence between the various types of system instability and the joint stiffness has been clarified. It turns out that relatively stiffer joint springs lead to flutter type instability. Also, it is beneficial to keep the shear spring stiffer in which case the critical force is relatively large. It will decline for a weaker shear spring irrespective of the bending spring rigidity.

(2) The joint internal damping together with the joint stiffness makes the type of instability and the critical forces change. The magnitude of the internal damping does not seem to affect the critical forces whenever the joint springs are relatively stiffer. For a relatively weaker bending spring, however, the critical force depends on the magnitude of the bending damping. Likewise, the shear joint damping affects the critical force when the shear springs are relatively weaker.

(3) Bending-flutter, post-flutter-divergence and folding instability at the joint appear as important instability types from the viewpoint of structural safety.

ACKNOWLEDGMENT

The first author, K. A. Mladenov, would like to express his heartfelt gratitude to the Japan Society for the Promotion of Sciences (JSPS) for the JSPS Long-Term Fellowship (FY 1995) to conduct research in Japan.

REFERENCES

1. T. R. BEAL 1965 *AIAA Journal* **3**, 486–495. Dynamic stability of a flexible missile under constant and pulsating thrusts.
2. G. Y. MATSUMOTO and C. D. MOTE 1972 *Transactions of the ASME*, *Journal of Dynamic Systems*, *Measurement and Control* **39**, 330–334. Time delay instabilities in large order systems with controlled follower forces.

3. Y. Park and C. D. Mote 1985 *Journal of Sound and Vibration* **98**, 247–256. The maximum controlled follower force on a free-free beam carrying a concentrated mass.
4. Y. Park 1985 *Proceedings of the JSME Vibration Conference* '85, 45–53. Dynamic stability of a free Timoshenko beam under controlled follower force.
5. J. J. Wu 1975 *Journal of Sound and Vibration* **42**, 45–52. On the stability of a free-free beam under axial thrust subjected to directional control.
6. J. J. Wu 1976 *AIAA Journal* **14**, 313–319. Missile stability using finite elements—an unconstrained variational approach.
7. J. J. Wu 1976 *Journal of Sound and Vibration* **49**, 141–147. On missile stability.
8. Y. Sugiyama, T. Katayama, H. Fukuda and C. Kar 1989 *Transactions of the JSME* **55**, 243–247. Effect of internal damping on the stability of free-free beams under an end thrust (in Japanese).
9. S.-H. Chen, Z.-H. Liu, W.-Z. Han and A.-J. Ma 1994 *AIAA Journal* **32**, 440–443. Determining free-free models from experimental data of constrained structures.
10. R. S. Barsoum 1971 *International Journal of Numerical Methods in Engineering* **3**, 63–87. Finite element method applied to the problem of stability of a non-conservative system.
11. V. V. Bolotin 1963 *Nonconservative Problems of Elastic Stability*. New York: Pergamon Press.
12. Y. Sugiyama and Ts. Sekiya 1970 *Journal of the JSME* **73**, 1238–1245. Stability problems of nonconservative elastic systems (in Japanese).
13. K. Sezawa 1927 *Tokyo Imperial University Scientific Reports* **3**, 43–53. On the decay of waves in visco-elastic solid bodies.

APPENDIX

Constituent Matrices for the Matrix Equation (8)

$$\mathbf{M}^{(i)} = \begin{bmatrix} 13/35N^4 & — & — & — \\ 11/210N^5 & 1/105N^6 & Sym & — \\ 9/70N^4 & 13/420N^5 & 13/35N^4 & — \\ -13/420N^5 & -1/140N^6 & -11/210N^5 & 1/105N^6 \end{bmatrix}^{(i)},$$

$$\mathbf{K}_1^{(i)} = \begin{bmatrix} 12 & & & \\ 6/N & 4/N^2 & Sym & \\ -12 & -6/N & 12 & \\ -6/N^2 & 2/N^2 & -6/N & 4/N^2 \end{bmatrix}^{(i)},$$

$$\mathbf{K}_2^{(i)} = \begin{bmatrix} (6(i-1)+3)/5 & & & \\ \left(\frac{i-1}{10}+\frac{1}{10}\right)\Big/N & \left(2\frac{i-1}{15}+\frac{1}{30}\right)\Big/N^2 & Symmetric & \\ -\frac{6(i-1)+3}{5} & \left(-\frac{i-1}{10}-\frac{1}{10}\right)\Big/N & \frac{6(i-1)+3}{5} & \\ \frac{i-1}{10N} & \left(-\frac{i-1}{30}-\frac{1}{60}\right)\Big/N^2 & -\frac{i-1}{10N} & \left(2\frac{i-1}{15}+\frac{1}{30}\right)\Big/N^2 \end{bmatrix}^{(i)},$$

$$\mathbf{L}_1^{(\mathrm{N})} = \begin{bmatrix} 0 & 0 & 0 & 0 \\ 0 & 0 & 0 & 0 \\ 0 & 0 & 0 & \pi^2 Q/N^3 \\ 0 & 0 & 0 & 0 \end{bmatrix},$$

$$\mathbf{C}^{(\mathrm{i})} = \gamma \int_0^1 (a_{\xi\xi} a'_{\xi\xi})^{(i)} \, \mathrm{d}\xi = \gamma \begin{bmatrix} 12 & & & \\ 6/N & 4/N^2 & Sym & \\ -12 & -6/N & 12 & \\ 6/N & 2/N^2 & -6/N & 4/N^2 \end{bmatrix}^{(i)}$$

$\mathbf{C}_{\mathrm{D1}}$, $\mathbf{C}_{\mathrm{D2}}$, $\mathbf{K}_{\mathrm{S1}}$ and $\mathbf{K}_{\mathrm{S2}}$ are given by the expressions

$$\mathbf{C}_{\mathrm{D1}} = (\delta_r/N^3) M_{\mathrm{C1}}$$

$$= \frac{\delta_r}{N} \{[a_\xi|_{(\xi=0)}^{(i)}][a'_\xi|_{\xi=0)}^{(i)}] + [a_\xi|_{(\xi=1)}^{(i-1)}][a'_\xi|_{(\xi=1)}^{(i-1)}] - [a_\xi|_{(\xi=0)}^{(i)}][a'_\xi|_{(\xi=1)}^{(i-1)}] - [a_\xi|_{(\xi=1)}^{(i-1)}][a'_\xi|_{(\xi=0)}^{(i)}]\},$$

$$\mathbf{M}_{\mathrm{C1}} = \left\{ \begin{array}{cc} & \begin{array}{ccccc} & & & 2i & 2i+2 \end{array} \\ \begin{array}{c} \\ 2i \\ \\ 2i+2 \\ \\ \end{array} & \begin{array}{c} \cdots \\ \\ \cdots \\ \\ \end{array} \begin{bmatrix} 0 & 0 & 0 & 0 & 0 \\ 0 & 1 & 0 & -1 & 0 \\ 0 & 0 & 0 & 0 & 0 \\ 0 & -1 & 0 & 1 & 0 \\ 0 & 0 & 0 & 0 & 0 \end{bmatrix} \end{array} \right\},$$

$$\mathbf{C}_{\mathrm{D2}} = \frac{\delta_s}{N^3} \{[a|_{(\xi=0)}^{(i)}][a'|_{(\xi=0)}^{(i)}] + [a|_{(\xi=1)}^{(i-1)}][a'|_{(\xi=1)}^{(i-1)}] - [a|_{(\xi=0)}^{(i)}][a'|_{(\xi=1)}^{(i-1)}] - [a|_{(\xi=1)}^{(i-1)}][a'|_{(\xi=0)}^{(i)}]\}$$

$$= \frac{\delta_s}{N^3} \left\{ \begin{array}{cc} & \begin{array}{ccccc} & & & 2i-1 & 2i+2 \end{array} \\ \begin{array}{c} \\ 2i-1 \\ \\ 2i+1 \\ \\ \end{array} & \begin{array}{c} \cdots \\ \\ \cdots \\ \\ \end{array} \begin{bmatrix} 0 & 0 & 0 & 0 & 0 \\ 0 & 1 & 0 & -1 & 0 \\ 0 & 0 & 0 & 0 & 0 \\ 0 & -1 & 0 & 1 & 0 \\ 0 & 0 & 0 & 0 & 0 \end{bmatrix} \end{array} \right\},$$

$$\mathbf{K}_{\mathrm{S1}} = \frac{\kappa_r}{N^3} \{[a_\xi|_{(\xi=0)}^{(i)}][a'_\xi|_{(\xi=0)}^{(i)}] + [a_\xi|_{(\xi=1)}^{(i-1)}][a'_\xi|_{(\xi=1)}^{(i-1)}] - [a_\xi|_{(\xi=0)}^{(i)}][a'_\xi|_{(\xi=1)}^{(i-1)}] - [a_\xi|_{(\xi=1)}^{(i-1)}][a'_\xi|_{(\xi=0)}^{(i)}]\}$$

$$= \frac{\kappa_r}{N^3} \left\{ \begin{array}{cc} & \begin{array}{ccccc} & & & 2i & 2i+2 \end{array} \\ \begin{array}{c} \\ 2i \\ \\ 2i+2 \\ \\ \end{array} & \begin{array}{c} \cdots \\ \\ \cdots \\ \\ \end{array} \begin{bmatrix} 0 & 0 & 0 & 0 & 0 \\ 0 & 1 & 0 & -1 & 0 \\ 0 & 0 & 0 & 0 & 0 \\ 0 & -1 & 0 & 1 & 0 \\ 0 & 0 & 0 & 0 & 0 \end{bmatrix} \end{array} \right\},$$

$$\mathbf{K}_{S2} = \frac{\kappa_s}{N^3}\left\{[a|^{(i)}_{(\xi=0)}][a'|^{(i)}_{(\xi=0)}] + [a|^{(i-1)}_{(\xi=1)}][a'|^{(i-1)}_{(\xi=1)}] - [a|^{(i)}_{(\xi=0)}][a'|^{(i-1)}_{(\xi=1)}] - [a|^{(i-1)}_{(\xi=1)}][a'|^{(i)}_{(\xi=0)}]\right\}$$

$$= \frac{\kappa_s}{N^3}\left\{\begin{array}{cc} & \begin{array}{ccccc} & & & 2i-1 & & 2i+2 & \\ & & & \vdots & & \vdots & \end{array} \\ \begin{array}{c} 2i-1 \\ \\ 2i+1 \end{array} \cdots & \left[\begin{array}{ccccc} 0 & 0 & 0 & 0 & 0 \\ 0 & 1 & 0 & -1 & 0 \\ 0 & 0 & 0 & 0 & 0 \\ 0 & -1 & 0 & 1 & 0 \\ 0 & 0 & 0 & 0 & 0 \end{array}\right] \end{array}\right\}.$$